Article

Flat-panel laser displays through large-scale photonic integrated circuits

Zhujun Shi[1,2], Risheng Cheng[1,2], Guohua Wei[1,2], Steven A. Hickman[1], Min Chul Shin[1], Peter Topalian[1], Lei Wang[1], Dusan Coso[1], Youmin Wang[1], Qingjun Wang[1], Brian Le[1], Lizzy Lee[1], Daniel Lopez[1], Yuhang Wu[1], Sean Braxton[1], Alexander Koshelev[1], Maxwell F. Parsons[1], Rahul Agarwal[1], Barry Silverstein[1], Yun Wang[1] & Giuseppe Calafiore[1✉]

Laser-based displays are highly sought after for their superior brightness and colour performance[1], especially in advanced applications such as augmented reality (AR)[2]. However, their broader use has been hindered by bulky projector designs and complex optical module assemblies[3]. Here we introduce a laser display architecture enabled by large-scale visible photonic integrated circuits (PICs)[4–7] to address these challenges. Unlike previous projector-style laser displays, this architecture features an ultra-thin, flat-panel form factor, replacing bulky free-space illumination modules with a single, high-performance photonic chip. Centimetre-scale PIC devices, which integrate thousands of distinct optical components on-chip, are carefully tailored to achieve high display uniformity, contrast and efficiency. We demonstrate a 2-mm-thick flat-panel laser display combining the PIC with a liquid-crystal-on-silicon (LCoS) panel[8,9], achieving 211% of the colour gamut and more than 80% volume reduction compared with traditional LCoS displays. We further showcase its application in a see-through AR system. Our work represents an advancement in the integration of nanophotonics with display technologies, enabling a range of new display concepts, from high-performance immersive displays to slim-panel 3D holography.

In the history of display technology, the shift from bulky cathode ray tube displays to compact flat-panel displays marked a pivotal moment. For nearly half a century, cathode ray tubes dominated the market until the advent of light-emitting diode (LED)-based flat-panel displays enabled a wave of portable devices, reshaping how we interact with visual technology in everyday life—from televisions to smartphones. Today, flat-panel displays are ubiquitous, yet the next leap forward—integrating laser technology into flat panels for the ultimate visual experience—remains a substantial challenge.

Lasers offer superior brightness and colour performance compared with conventional LED-based displays[1]. The high directionality of laser light affords projection of images with high peak brightness, which also enables display operation at lower duty cycle, critical for suppressing motion artefacts[10]. Their narrow spectrum provides more saturated colours, resulting in wider colour gamut. Their polarized output reduces losses in display systems with polarization-sensitive components, leading to improved efficiency. These characteristics are particularly valuable for immersive experiences, such as AR, virtual reality (VR) and other high-performance display systems.
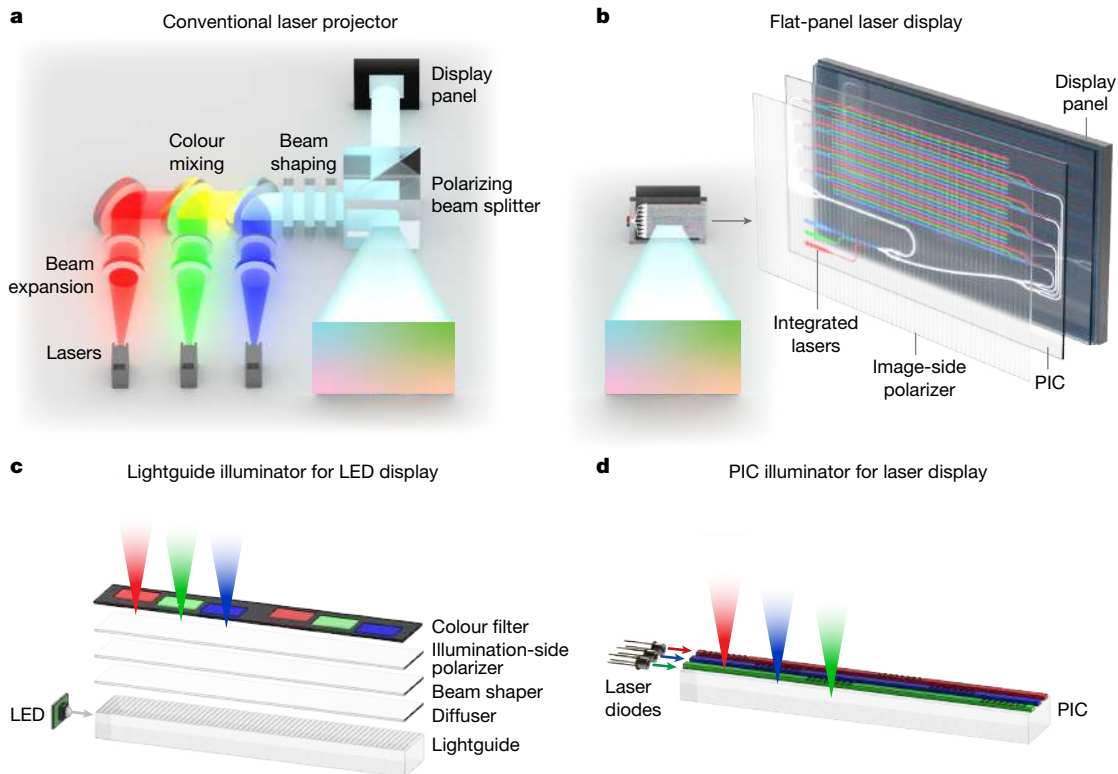
However, despite these benefits, present laser displays are largely confined to bulky projector formats, such as those used in movie theatres[3], in which complex optical systems are used to deliver laser light to a screen. As shown in Fig. 1a, a typical laser projector consists of several optical elements for beam expansion, beam shaping, colour mixing, polarization control and other functions. Moreover, a notable volume for free-space propagation is required to expand narrow laser beams over a large display area. Miniaturized scanning-based laser displays have been demonstrated but they suffer from the intrinsic speed–resolution trade-off, various visual artefacts and also complexity in display driving and rendering[11,12]. Several attempts have been made to develop flat-panel laser displays, but they require complicated laser arrays[13] or low-throughput fabrication methods[14], greatly limiting their performance and scalability.

The challenge of transitioning laser projectors to flat panels lies in the precise control required to manage laser light. Most LED-based flat-panel displays, for example, liquid-crystal displays (LCDs)[15], use a 'diffuse and filter' approach, in which light is first homogenized by means of random scattering in a thin lightguide and then passes through several layers of filters, such as pixelated colour filters, polarizers and angular filters to achieve the desired light output (Fig. 1c). This approach, however, cannot readily be applied to laser displays without negating the benefits of high directionality, polarization and colour purity. Instead, laser displays require precise photon delivery, directing light exactly where it is needed with the right spatial, angular, spectral and polarization characteristics, to maintain their performance advantages. Achieving this level of precision necessitates complex bulky optical systems when using conventional optics, resulting in large projector systems.

Here we introduce a new laser display architecture that features a slim, flat-panel form factor (Fig. 1b), overcoming the long-standing

a Conventional laser projector

Display panel

Colour mixing

Beam shaping

Polarizing beam splitter

Beam expansion

Lasers

b Flat-panel laser display

Display panel

Integrated lasers

Image-side polarizer

PIC

c Lightguide illuminator for LED display

Colour filter
Illumination-side polarizer
Beam shaper
Diffuser
Lightguide

LED

d PIC illuminator for laser display

Laser diodes

PIC

Fig. 1 | Concept of flat-panel laser displays. a, Schematic of a conventional laser projector using free-space illumination. It consists of laser sources, collimating lenses, dichroic mirrors, beam-shaping elements, a polarizing beam splitter and a display panel. **b**, Schematic of the proposed flat-panel laser display. A PIC is used to replace the free-space illumination module and integrated directly onto the display panel, achieving a compact flat-panel form factor. **c**,**d**, Comparison of LED and laser illumination. **c**, Typical LED lightguide illuminators, or backlights, use several layers of diffusers and light filters to tailor the spatial, angular, spectral and polarization characteristics of light, resulting in low optical efficiency. **d**, The PIC illuminator eliminates the need for lossy diffusers and filters by guiding and tailoring the light characteristics on-chip.

trade-off between size and performance in laser displays by using a large-scale visible PIC[4–7]. We integrate thousands of components with different optical functions on a single photonic chip, carefully designed to cohesively control the red, green and blue (RGB) colour channels to meet the high demands of advanced display applications. The PIC functions similarly to the lightguide in LCDs—expanding light and tailoring its spatial, angular, spectral and polarization characteristics according to the display system requirements. However, the working principle is very different: it uses a 'guide and select' approach rather than the 'diffuse and filter' method. Light expansion is achieved through on-chip guiding and splitting, not random diffusing; angular spread is controlled by engineered grating emitters, not beam-shaping filters; polarization and colour purity are maintained and the light is outcoupled selectively so that no more colour filters or polarizers are needed on the illumination side (Fig. 1d). Our architecture also offers new capabilities, such as on-demand chief ray angle adjustment across the display, enabling co-design of the illumination module and optical system for optimal overall display performance. Fabrication of the PIC devices is based on standard complementary metal–oxide–semiconductor (CMOS)-compatible processes, making it scalable for mass production. Laser-to-PIC integration[16,17], already established in the telecommunications industry, can also be adapted for the visible regime.

Our PIC illumination architecture provides a versatile platform for existing and emerging display technologies. It is compatible with a variety of display panels, including LCDs, LCoS displays[8,9] and digital light processing (DLP) displays[18], and has a wide range of applications, from smartphone displays to AR glasses[2] to emerging holographic displays[19–25]. As a proof of concept, here we demonstrate a flat-panel

laser display based on PICs and LCoS for AR applications, for which compactness, high efficiency and high brightness are crucial.

Display architecture

The proposed flat-panel laser display uses a non-emissive display configuration. Flat-panel displays generally fall into two categories[26]: emissive displays, such organic LEDs (known as OLEDs), which generate light directly from each pixel; and non-emissive displays, such as LCDs, in which the pixels rely on external illumination rather than emitting light themselves. Here we choose a non-emissive configuration to avoid the complexity of integrating and controlling a large number of laser diodes on a dense, micron-scale pixel lattice. There are three key modules in non-emissive displays: the light source, the illumination unit and the light modulation device. Here we use RGB semiconductor laser diodes, a PIC illuminator and a colour-sequential LCoS display panel, respectively (Fig. 2a), to demonstrate this concept and its application for AR glasses.

The display stack is illustrated in Fig. 2a. The PIC device is placed over the LCoS cover glass, with a polarizer film laminated on top of the PIC device for image formation. LCoS is a reflective display that modulates the polarization on reflection by changing the liquid crystal orientation at each pixel[8,27] (Fig. 2b). Through polarization filtering, the polarizer translates modulated polarization into modulated intensity, forming an image. To maximize the display resolution, we use a colour-sequential LCoS without RGB subpixels—the full-colour image is created by showing the RGB colour channels in rapid succession over a frame time. For quick prototyping, off-the-shelf fibre-coupled lasers are used, combined off-chip and coupled to the PIC device through a
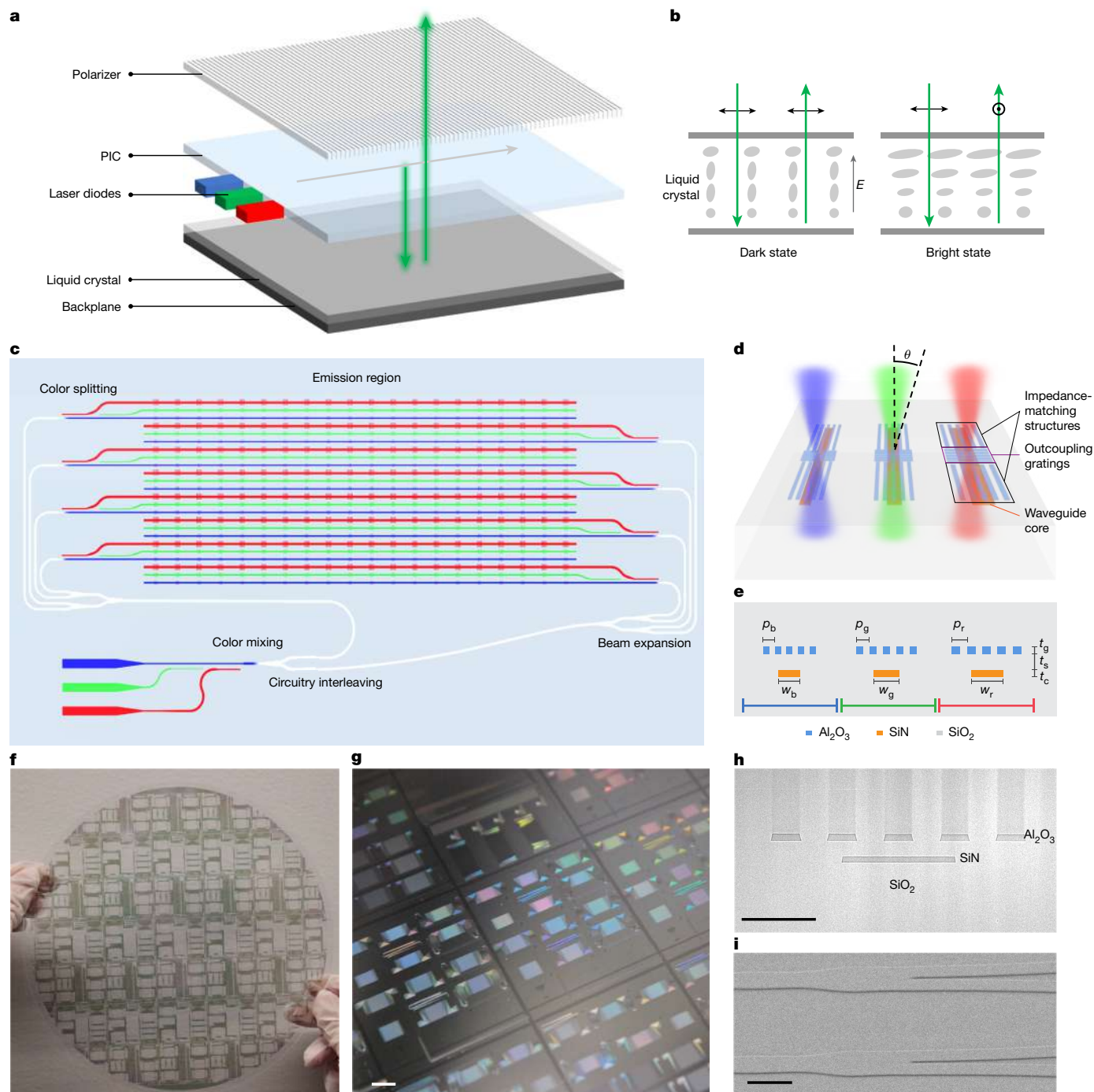
Fig. 2 | Device design and fabrication. a, Schematic of the flat-panel laser display stack. The PIC is placed between a LCoS display panel and a polarizer. It expands the laser inputs over an area to illuminate the LCoS panel. The LCoS panel then reflects the light and modulates its polarization spatially, which is converted into intensity modulation after passing through the polarizer. **b**, Polarization rotation at the liquid crystal layer. In the dark state, the liquid crystal molecules are aligned vertically, leaving polarization unchanged, so the reflected light is blocked by the cross-polarizer. In the bright state, the liquid crystal molecules form a twisted structure that rotates the polarization of light by 90° on reflection, resulting in a bright state. **c**, Schematic of the PIC layout. **d**, Zoom-in view of the grating emitters. The RGB emitters are placed side by side, sharing the same core and grating layers. For each emitter, the grooves

transverse to the core waveguide are short gratings for light extraction. The grating pitch determines the emission direction and the grating length determines the divergence angle. The grooves parallel to the core waveguide are impedance-matching structures. They are introduced between adjacent emitters to minimize the scattering loss. **e**, Cross-section view of the PIC stack. It consists of a 50-nm SiN core (t_c), a 170-nm SiO$_2$ spacer (t_s) and a 55-nm AlO$_x$ grating layer (t_g). The core waveguide widths ($w_{r/g/b}$) and the grating pitches ($p_{r/g/b}$) are optimized separately for R, G and B. **f**, Optical image of a 200-mm-diameter PIC wafer. **g**, Optical image of the device before the wafer is transferred to the glass substrate (see Methods). **h**, SEM image of the cross-sectional layer stack. **i**, SEM image of the Y-splitters. Scale bars, 5 mm (**g**), 500 nm (**h**), 3 μm (**i**).

single fibre attachment. Direct edge-coupling or flip-chip bonding of the lasers to the PIC and on-chip colour mixing is discussed in Supplementary Information Section 3.

The display operation starts from light generation at the RGB laser diodes, which are turned on sequentially in synchronization with the LCoS colour frame transition. Each laser is operated with a specific
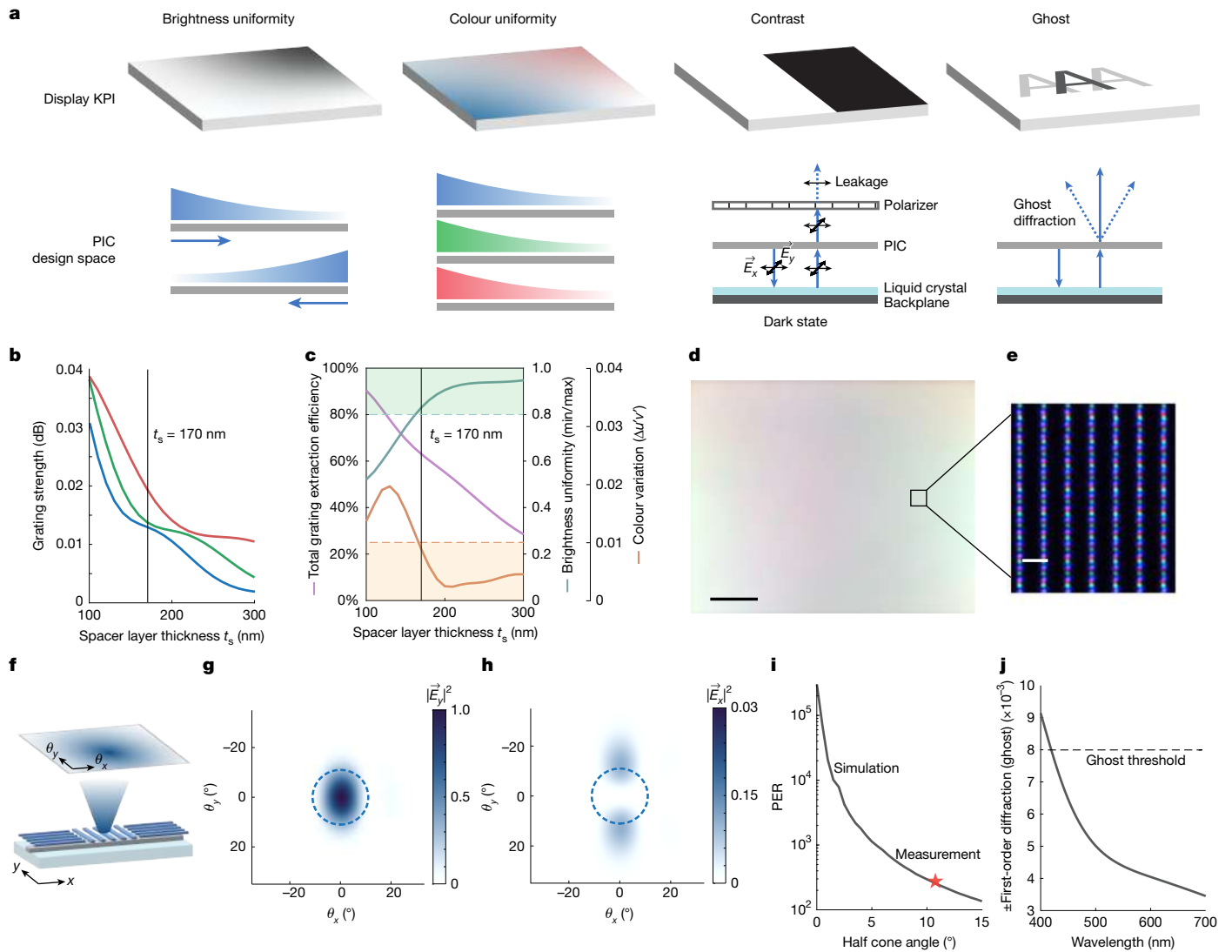
Fig. 3 | Display performance analysis. a, Key display performance factors and the corresponding PIC design space. **b**, Simulated grating strength as a function of the SiO$_2$ spacer layer thickness t_s for R, G and B. The SiN core thickness and the AlO$_x$ grating layer thickness are fixed at 50 nm and 55 nm, respectively. **c**, Simulated brightness uniformity, colour uniformity and light extraction efficiency as a function of t_s. The green shading represents the allowable range for brightness uniformity, min/max > 0.8. The orange shading represents the allowable range for colour uniformity, Δ$u'v'$ < 0.01. **d**, Measured uniformity map of a fabricated PIC illuminator. The device size is 6.0 mm by 4.8 mm. **e**, Zoom-in view of the PIC emitters. **f**, Schematic of the grating emitters. **g**, Simulated far-field intensity profiles for Y-polarization (transverse to the polarizer transmission axis). The dashed circle represents the target cone angle. **h**, Simulated far-field intensity profiles for X-polarization (parallel to the polarizer transmission axis). **i**, Line, simulated PER as a function of the light collection half angle. Star, measured PER at 11° half cone angle. **j**, Simulated diffraction efficiency into the ghost orders. KPI, key performance indicator. Scale bars, 1 mm (**d**), 20 μm (**e**).

pulse width and duty cycle to optimize the spectrum and laser wall plug efficiency. To minimize the device footprint, we first combine the RGB colours, either on-chip or off-chip, and expand them using a shared set of cascaded Y-splitters (Fig. 2c). Following the expansion, the white light is separated back into RGB colours through coarse-wavelength multiplexers. Here colour splitting is needed for individual control of the R, G and B emission profiles. In the emission region, light is extracted by means of arrays of pixelated grating couplers (Fig. 2d). Each grating emitter is designed to be 1–2 μm in length to produce a finite diffraction cone angle, which can be matched with the numerical aperture (NA) of the viewing optics (Fig. 2d,e). The emission area is slightly oversized compared with the active area of the LCoS panel to avoid brightness roll-off at the edges. Finally, the illumination light is modulated by the LCoS panel on reflection and forms an image after the polarizer. It is also worth noting that the grating emitters emit light in both directions. To further enhance the efficiency of light

use, we use reflective-type polarizers to recycle light emitted in the opposite direction, redirecting it back towards the LCoS side (see Supplementary Information Section 3). Figure 2f–i shows the optical images of the wafer and scanning electron microscopy (SEM) images of the PIC stack and Y-splitters. More details on the PIC fabrication process can be found in Methods and Supplementary Information Section 1.

Design principle

Our design carefully manages the trade-offs in the four key performance metrics for the PIC illuminator: uniformity, polarization extinction ratio, transparency and efficiency, which correspond directly to the critical display performance factors: display uniformity, contrast ratio, ghosting and power consumption, respectively (Fig. 3a). Here uniformity includes both brightness and colour.

Article

One notable trade-off is between brightness uniformity and light extraction efficiency: stronger gratings increase extraction efficiency but degrade uniformity owing to exponential intensity decay along the waveguides. To overcome this, we introduce a new optical circuitry design—spatial interleaving of waveguide circuits. As illustrated in Fig. 2c, light is split on-chip and fed from opposite directions through two sets of Y-splitters. This creates a compensatory effect, maintaining uniform illumination despite the monotonic decay in each direction (Fig. 3a).

We achieve high colour uniformity by optimizing the PIC layer stack and grating strength for each colour. According to the Born approximation, the grating outcoupling efficiency is proportional to the mode intensity at the grating structures. Therefore, to realize good colour uniformity requires matching the grating efficiency for R, G and B, which—in turn—requires engineering their mode profiles. To achieve this, we use a three-layer PIC design—the gratings are patterned in a separate aluminium oxide (AlO_x) layer above the silicon nitride (SiN) core waveguiding layer, with a silicon dioxide (SiO_2) spacer layer in between (Fig. 2d,e). Compared with the conventional direct waveguide etching, the three-layer stack offers more design degrees of freedom to tailor the mode and grating interaction as a function of wavelength.

The trade-off between uniformity and efficiency is shown in Fig. 3b,c, with a specific focus on the spacer layer thickness t_s for illustration purposes. Following display industry convention, brightness uniformity is defined by the min/max brightness ratio, which must exceed 80%. Colour uniformity, measured by $\Delta u'v'$ (deviation from the white point)[28], must remain below 0.01. We can clearly see the design trade-offs: the efficiency and brightness uniformity trend oppositely with t_s, whereas colour uniformity is optimized at t_s around 200 nm. In our device, we choose $t_s = 170$ nm as it offers the overall best performance: it can meet the uniformity requirements while achieving a high light extraction efficiency of 60%. More details on the further potential trade-off optimization on the uniformity are presented in Supplementary Information Sections 3 and 4.

The polarization extinction ratio (PER), critical for display contrast, is optimized by using single-mode waveguides and polarization-selective gratings. As shown in Fig. 3a, the illumination polarization is designed to be orthogonal to the transmission axis of the polarizer. Any cross-polarization will lead to dark state light leakage and thus low display contrast. Here we achieve an on-axis PER greater than 10,000:1 in simulation (Fig. 3i) by carefully ensuring high polarization selectivity in the waveguides and grating couplers. Note that the PER decreases at oblique angles, creating a trade-off between contrast and the NA of the optical system (Fig. 3f–h).

Owing to the reflective nature of the LCoS, light passes through the PIC illuminator again on reflection from the LCoS panel. This adds another key requirement—the PIC must be highly transparent to avoid any ghosting or image quality degradation. Note that the transparency of the PIC in the imaging path and high efficiency in the illumination path do not violate reciprocity, as the emitted light is diverging. On reflection, the beam size has grown far beyond the effective grating cross-section. In fact, the re-interaction of light with the PIC is dominated by diffraction at the ridge waveguides, rather than at the gratings. Figure 3j shows the simulated diffraction efficiency integrated over the collection cone angle. Because both SiN and AlO_x layers are optically thin, the diffraction efficiency from the PIC waveguides is less than 0.8% across the spectrum of interest, meeting the requirement of typical AR applications.

Finally, we optimize the optical efficiency of the PIC device by refining all components, minimizing propagation and bending losses in waveguides, insertion losses at Y-splitters and coarse-wavelength multiplexers, optimizing laser-to-PIC coupling efficiencies, designing impedance mismatches at grating emitters and maximizing grating extraction efficiency (see Supplementary Information Sections 2–4). A low-loss SiN waveguide platform has been previously demonstrated and reported from near-infrared to telecommunications wavelength regimes[29–31]. In this work, we extend these boundaries further by achieving very low propagation losses across the entire visible spectrum with a small device footprint. We measured waveguide losses of 0.1 dB cm^{-1}, 0.3 dB cm^{-1} and 1.1 dB cm^{-1} at R, G and B wavelengths (635 nm, 520 nm and 450 nm, respectively), which are lower than those previously reported from SiN photonic foundries[6,32]. The SiN core thickness is carefully designed to minimize bending and insertion losses, while ensuring single-mode operation across all colours and maintaining compactness. The Y-splitters are inversely designed for minimal insertion loss and broadband performance. With a series of comprehensive designs and further process optimizations, we anticipate that our architecture could achieve up to almost tenfold improvement in optical efficiency over conventional LCoS projectors (see Supplementary Information Section 5).

Performance evaluation

We have evaluated the performance of our flat-panel laser display architecture in a series of experiments, starting with the characterization of the stand-alone PIC illuminator, followed by the assembled flat-panel laser display and, finally, a full AR system.

High illumination uniformity is achieved experimentally. Figure 3d shows the measured illumination field before integrating with the LCoS. The PIC emission area is 6.0 mm by 4.8 mm, with the long axis along the waveguides. Owing to the interleaved light propagation, the illumination is brighter towards the edges and dimmer towards the centre. The measured brightness uniformity (min/max) is 71%, slightly lower than the design value, owing to the layer thickness variation from fabrication shift, and a good colour uniformity with $\Delta u'v' < 0.01$ is achieved. Note that the human perception of colour variation depends strongly on the spatial frequency, that is, slowly varying colour change across a large field of view (FoV) is much less noticeable. Therefore, although the colour variation is visible in the figure, it is perceptually less obvious when observed over the designed 30° by 40° FoV. A zoomed-in view of the PIC is shown in Fig. 3e, illustrating the individual grating emitters. Note that, because of circuitry interleaving, the emitter lattice spacing along waveguides is twice that in the direction transverse to waveguides.

We have also measured the illumination PER (Fig. 3i). Owing to limitations in the characterization set-up, the measured PER is integrated over a NA of 0.2. A spatial variation of the measured PER across the PIC device is observed, mainly because of the unwanted light scattering at the edge-coupling region (Supplementary Information Section 4). Away from the edge coupler is an illumination contrast of more than 250:1 at NA ≈ 0.2, in agreement with the simulation.

Next, we evaluated the display performance after the PIC–LCoS integration. Figure 4a shows a fully functional display assembly with a compact form factor and high brightness. The LCoS panel used here has a 4.5-µm pixel pitch with full high definition (1,920 × 1,080) resolution and operates at 180 Hz frame rate per colour channel.

One advantage of laser displays is wider colour gamut. As we use narrowband prime-colour lasers, the colour gamut is wider than any other LED-based displays (Fig. 4b). It provides 211% gamut ratio and full coverage of sRGB/BT.709, the standard for high-definition TV defined by the International Telecommunication Union (ITU). As a comparison, our display encompasses 74% of the visible colours specified by the CIELAB colour space, whereas the standard Adobe RGB colour space[33] covers only 52% and sRGB[34] covers only 36%.

The display performance under direct view is shown in Fig. 4c–f. An eyepiece is used to magnify the displayed image (see Methods). The image blur towards the edge is because of the aberrations of the eyepiece lens and not from the display. The assembled display sequential
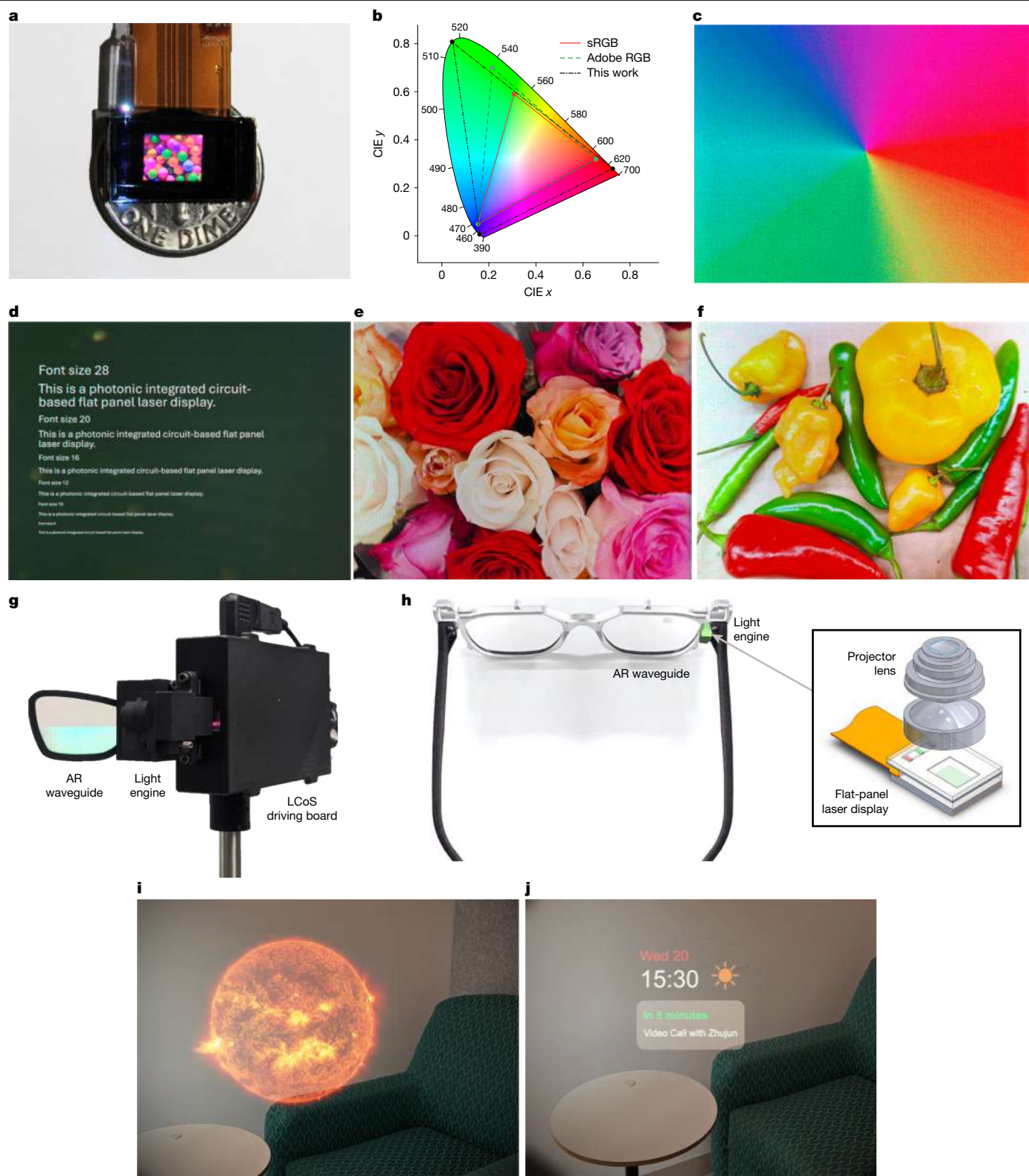
Fig. 4 | Measured display images under direct view and AR configurations. **a**, The assembled flat-panel laser display shown on top of a dime coin. A fibre is attached to the PIC for light input. The flex cable is for LCoS control. The light sources and laser controllers are not shown in the photo. **b**, Colour performance of this work in comparison with standard colour spaces. **c**–**f**, Measured display images. **g**, Photo of the handheld AR set-up used in the experiment. **h**, Conceptual visualization of an AR system integrated with a form-factor-optimized flat-panel laser display. **i**,**j**, Images captured by a camera at the eye position of the AR set-up in panel **g**, showing the displayed virtual objects and real world of an office. Image credit: NASA.

contrast is around 40:1, much lower than the illumination PER. This is limited by both the LCoS panel contrast and the alignment error between the PIC, LCoS and the polarizer film, which was introduced manually for this demonstration. In actual manufacturing, this issue can be mitigated by a more precise alignment process based on optimized alignment marks.

a

Display content   Global illumination   Display content   Zonal illumination

b

3D image volume
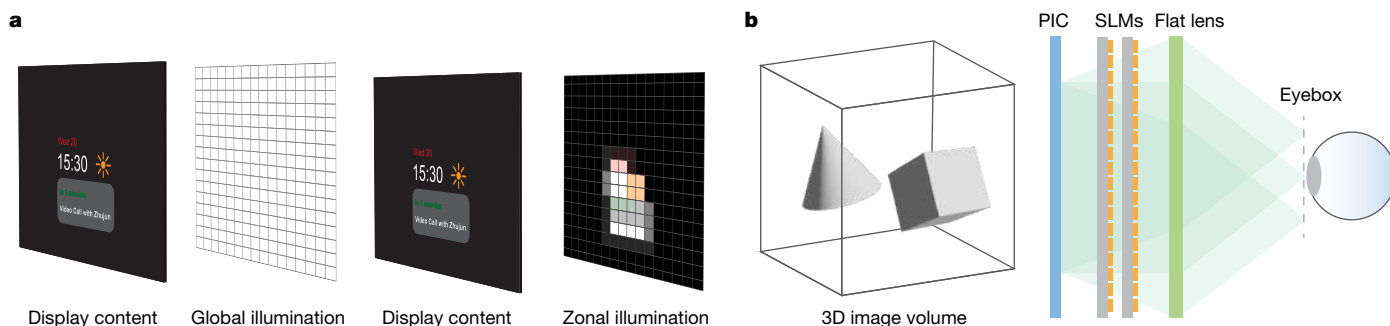
Fig. 5 | New display concepts enabled by PICs. a, Concept of zonal illumination. Zonal illumination can enhance image contrast and efficiency by turning on the illumination only where needed. It can be realized by using active PIC modulators. **b**, Schematic of a PIC-enabled holographic display. The PIC provides a tailored illumination field, which feeds into one or several layers of spatial light modulators (SLMs) for hologram generation. A flat lens, such as a holographic optical element, is then used to project and magnify the image.

A compact and efficient display engine is particularly important for AR glasses, given their tight space and power budget limited by the glass size and weight. Here we demonstrate the PIC laser display performance at a system level by pairing it with an off-the-shelf pupil-replicating AR geometrical glass (Fig. 4g). Light from the flat-panel laser display is first collimated by a custom-made lens module (Supplementary Information Section 6) and then coupled to the input pupil of the AR lightguide. The exit pupil is expanded through several total internal reflections inside the glass plate (Supplementary Information Section 9). The present demonstration is a handheld AR set-up with the projector supporting 50° diagonal FoV. The volume mainly comes from the large off-the-shelf LCoS display driving board and can be miniaturized substantially with a customized application-specific integrated circuit (ASIC)-based driver. With better integration and packaging, the light engine size can be reduced to less than 1 cubic centimetre (Supplementary Information Sections 6 and 12), enabling ultra-compact and lightweight AR experience (Fig. 4h). Several types of AR use case are demonstrated. Figure 4i,j demonstrates the mixed-reality experience in which the virtual images are blended seamlessly with the real-world scene in an office environment. Note that the speckles are much less noticeable after the AR lightguide, partially because of the reduced additive contrast with the see-through background.

Discussion

Realizing the full potential of PIC laser displays still faces several challenges. First is the laser speckle. Speckles are a known issue in laser displays[1]. Here we observe them as granular patterns in the image, resulting from the interference of different PIC emitters on the LCoS plane. As a first proof-of-principle demonstration, no further despeckling method is implemented in the present device. We measured around 20% speckle contrast with a 1-nm-bandwidth single-mode laser, exceeding the typical perception threshold of 4% (ref. 35). Several mitigation methods, such as wavelength or polarization diversity[36], dynamic diffusers[37] and microlens arrays[38], have been proposed and tested in existing laser projectors and can be adapted to the PIC laser displays. Further discussion on despeckling can be found in Supplementary Information Section 13.

Another key challenge is light source integration and packaging. Although laser integration is mature in silicon photonics for telecommunications wavelengths, the integration of RGB laser diodes with visible photonics is still at an early stage[39]. We have demonstrated direct laser–PIC edge coupling at a prototype level through active alignment (Supplementary Information Section 10). For mass production, die-to-wafer flip-chip bonding can be used as a cost-effective scalable manufacturing path and recent progress on heterogenous visible laser integration with SiN photonics provided another possibility on this avenue[40].

For AR application specifically, there is a challenge of the power waste and contrast degradation for sparse content in many use cases, such as depicted in Fig. 4i,j. At present, the PIC illuminator can only be turned on and off globally, leading to unfavourable power consumption when only a small portion of the LCoS display is on[41]. To further improve the illumination efficiency, active PIC modulation[4,42–45] might be used to control different illumination regions independently (Fig. 5a), a concept similar to local dimming in LCDs[46].

Beyond AR/VR, the PIC illuminator serves as an enabling platform for a broad range of new display concepts, including slim-panel holographic displays[19,20], high-resolution light field displays[47], pupil-steered displays[48] and many more. As an example, Fig. 5b illustrates a potential application of PICs in holographic displays, in which the PIC illuminator is integrated with spatial light modulators and a holographic pancake lens[49]. Unlike previous holographic displays, which rely on simple plane-wave incidence[22], the PIC could provide a tailored illumination field co-optimized with the holographic display system, achieving unprecedented compactness, brightness and immersiveness.

This work introduces large-scale visible PICs as a powerful platform for compact and efficient laser illumination. We demonstrate a flat-panel laser display architecture that achieves substantial miniaturization, paving the way for advanced applications in AR and beyond. We believe that our work could facilitate more innovations that make use of advanced nanophotonics in the display industry, driving advancements in next-generation visual technologies.

Online content

Any methods, additional references, Nature Portfolio reporting summaries, source data, extended data, supplementary information, acknowledgements, peer review information; details of author contributions and competing interests; and statements of data and code availability are available at https://doi.org/10.1038/s41586-025-09107-7.

1. Chellappan, K. V., Erden, E. & Urey, H. Laser-based displays: a review. *Appl. Opt.* **49**, F79–F98 (2010).
2. Xiong, J., Hsiang, E.-L., He, Z., Zhan, T. & Wu, S.-T. Augmented reality and virtual reality displays: emerging technologies and future perspectives. *Light Sci. Appl.* **10**, 216 (2021).
3. Silverstein, B. D., Kurtz, A. F., Bietry, J. R. & Nothhard, G. E. 25.4: A laser-based digital cinema projector. *SID Symp. Dig. Tech. Pap.* **42**, 326–329 (2011).
4. Shin, M. C. et al. Chip-scale blue light phased array. *Opt. Lett.* **45**, 1934–1937 (2020).
5. Poulton, C. V. et al. Large-scale silicon nitride nanophotonic phased arrays at infrared and visible wavelengths. *Opt. Lett.* **42**, 21–24 (2017).
6. Sacher, W. D. et al. Visible-light silicon nitride waveguide devices and implantable neurophotonic probes on thinned 200 mm silicon wafers. *Opt. Express* **27**, 37400–37418 (2019).
7. Calafiore, G. et al. Holographic planar lightwave circuit for on-chip spectroscopy. *Light Sci. Appl.* **3**, e203 (2014).

8. Zhang, Z., You, Z. & Chu, D. Fundamentals of phase-only liquid crystal on silicon (LCOS) devices. *Light Sci. Appl.* **3**, e213 (2014).
9. Huang, Y., Liao, E., Chen, R. & Wu, S.-T. Liquid-crystal-on-silicon for augmented reality displays. *Appl. Sci.* **8**, 2366 (2018).
10. Hoffman, D. M. & Lee, G. Temporal requirements for VR displays to create a more comfortable and immersive visual experience. *Inf. Disp.* **35**, 9–39 (2019).
11. Pohl, L. et al. Challenges and Opportunities Applying Laser Beam Scanning Displays Based on Biaxial Resonantly Operated MEMS Scanners. In *Proc. 2024 IEEE International Conference on Metrology for eXtended Reality, Artificial Intelligence and Neural Engineering (MetroXRAINE)* 976–981 (IEEE, 2024).
12. Reitterer, J. et al. Ultra-compact micro-electro-mechanical laser beam scanner for augmented reality applications. In *Proc. Optical Architectures for Displays and Sensing in Augmented, Virtual, and Mixed Reality (AR, VR, MR) II*, Vol. 11765, 33–43 (SPIE, 2021).
13. Komura, S., Onoda, K., Kijima, H. & Okuda, K. A laser backlight liquid crystal display with a narrow bezel. In *Proc. Ultra-High-Definition Imaging Systems III*, Vol. 11305, 10–19 (SPIE, 2020).
14. Vasconcelos, R., Zeuner, J. & Greganti, C. Laser light field display. In *Proc. Advances in Display Technologies XII*, Vol. 12024, 33–41 (SPIE, 2022).
15. Yang, D.-k. & Wu, S.-T. in *Fundamentals of Liquid Crystal Devices* 2nd edn, 213–233 (Wiley, 2014).
16. Tanaka, S. et al. High-output-power, single-wavelength silicon hybrid laser using precise flip-chip bonding technology. *Opt. Express* **20**, 28057 (2012).
17. Theurer, M. et al. Flip-chip integration of InP to SiN photonic integrated circuits. *J. Light. Technol.* **38**, 2630–2636 (2019).
18. Kessel, P. F. V., Hornbeck, L. J., Meier, R. E. & Douglass, M. R. A MEMS-based projection display. *Proc. IEEE* **86**, 1687–1704 (2021).
19. An, J. et al. Slim-panel holographic video display. *Nat. Commun.* **11**, 5568 (2020).
20. Gopakumar, M. et al. Full-colour 3D holographic augmented-reality displays with metasurface waveguides. *Nature* **629**, 791–797 (2024).
21. Notaros, J., Raval, M., Notaros, M. & Watts, M. R. Integrated-phased-array-based visible-light near-eye holographic projector. In *Proc. 2019 Conference on Lasers and Electro-Optics (CLEO)* 1–2 (IEEE, 2019).
22. Kim, J. et al. Holographic glasses for virtual reality. In *ACM SIGGRAPH 2022 Conference Proceedings* 1–9 (ACM, 2022).
23. Panuski, C. L. et al. A full degree-of-freedom spatiotemporal light modulator. *Nat. Photon.* **16**, 834–842 (2022).
24. Jabbireddy, S., Zhang, Y., Peckerar, M., Dagenais, M. & Varshney, A. Sparse nanophotonic phased arrays for energy-efficient holographic displays. In *Proc. 2022 IEEE Conference on Virtual Reality and 3D User Interfaces (VR)* 553–562 (IEEE, 2022).
25. Jang, C., Bang, K., Chae, M., Lee, B. & Lanman, D. Waveguide holography for 3D augmented reality glasses. *Nat. Commun.* **15**, 66 (2024).
26. Lee, J.-H., Cheng, I.-C., Hua, H. & Wu, S. *Introduction to Flat Panel Displays* 2nd edn, 15–37 (Wiley, 2020).
27. Wu, S.-T. & Wu, C.-S. Mixed-mode twisted nematic liquid crystal cells for reflective displays. *Appl. Phys. Lett.* **68**, 1455–1457 (1996).
28. Robertson, A. R. The CIE 1976 color-difference formulae. *Color Res. Appl.* **2**, 7–11 (1977).
29. Bryant, A. et al. Ultra-low-loss on-chip resonators with sub-milliwatt parametric oscillation threshold. *Optica* **4**, 619–624 (2017).
30. Liu, J. et al. High-yield, wafer-scale fabrication of ultralow-loss, dispersion-engineered silicon nitride photonic circuits. *Nat. Commun.* **12**, 2236 (2021).
31. Tran, M. A. et al. Extending the spectrum of fully integrated photonics to submicrometre wavelengths. *Nature* **610**, 54–60 (2022).
32. Smith, J. A., Francis, H., Navickaite, G. & Strain, M. J. SiN foundry platform for high performance visible light integrated photonics. *Opt. Mater. Express* **13**, 458 (2023).
33. International Organization for Standardization (ISO).ISO 12640-4:2011 Graphic technology — Prepress digital data exchange. Part 4: Wide gamut display-referred standard colour image data [Adobe RGB (1998)/SCID].
34. International Organization for Standardization (ISO). ISO 12640-2:2004(en). Graphic technology — Prepress digital data exchange — Part 2: XYZ/sRGB encoded standard colour image data (XYZ/SCID).
35. Roelandt, S. et al. Human speckle perception threshold for still images from a laser projection system. *Opt. Express* **22**, 23965–23979 (2014).
36. Tran, T.-T.-K., Svensen, Ø., Chen, X. & Akram, M. N. Speckle reduction in laser projection displays through angle and wavelength diversity. *Appl. Opt.* **55**, 1267–1274 (2016).
37. Kuratomi, Y. et al. Speckle reduction mechanism in laser rear projection displays using a small moving diffuser. *J. Opt. Soc. Am. A* **27**, 1812–1817 (2010).
38. Mizuyama, Y., Harrison, N. & Leto, R. Despeckling fly's eye homogenizer for single mode laser diodes. *Opt. Express* **21**, 9081–9090 (2013).
39. Franken, C. A. A. et al. Hybrid-integrated diode laser in the visible spectral range. *Opt. Lett.* **46**, 4904–4907 (2021).
40. Zhang, Z. et al. Photonic integration platform for rubidium sensors and beyond. *Optica* **10**, 752–753 (2023).
41. Peng, F. et al. 19-1: *Invited Paper*: Zonal illuminated non-emissive displays for AR glass. *SID Symp. Dig. Tech. Pap.* **55**, 220–222 (2024).
42. Notaros, M. et al. Integrated visible-light liquid-crystal-based phase modulators. *Opt. Express* **30**, 13790–13801 (2022).
43. Renaud, D. et al. Sub-1 Volt and high-bandwidth visible to near-infrared electro-optic modulators. *Nat. Commun.* **14**, 1496 (2023).
44. Dong, M. et al. High-speed programmable photonic circuits in a cryogenically compatible, visible–near-infrared 200 mm CMOS architecture. *Nat. Photon.* **16**, 59–65 (2022).
45. Xue, S. et al. Full-spectrum visible electro-optic modulator. *Optica* **10**, 125–126 (2023).
46. Chen, H., Sung, J., Ha, T. & Park, Y. Locally pixel-compensated backlight dimming on LED-backlit LCD TV. *J. Soc. Inf. Disp.* **15**, 981–988 (2007).
47. Yamaguchi, M. Light-field and holographic three-dimensional displays [Invited]. *J. Opt. Soc. Am. A* **33**, 2348–2364 (2016).
48. Ratnam, K., Konrad, R., Lanman, D. & Zannoli, M. Retinal image quality in near-eye pupil-steered systems. *Opt. Express* **27**, 38289–38311 (2019).
49. Maimone, A., Georgiou, A. & Kollin, J. S. Holographic near-eye displays for virtual and augmented reality. *ACM Trans. Graph.* **36**, 1–16 (2017).

Article

Methods

Device fabrication and integration

The PIC device is fabricated in a 200-mm (8-inch) CMOS foundry. The fabrication process begins with 200-mm silicon (Si) wafers coated with a 2.5-μm-thick thermal oxide (SiO_2) layer, followed by the deposition and patterning of a low-pressure chemical vapour deposition silicon nitride (SiN) layer, serving as the core waveguide. Deep-ultraviolet lithography and reactive ion etching are used for this patterning. Subsequently, a spacer SiO_2 layer is deposited over the SiN and planarized using chemical-mechanical polishing. Aluminium oxide (AlO_x) is then deposited through atomic layer deposition and patterned to form grating emitters. Another SiO_2 layer is deposited and planarized thereafter. Titanium nitride (TiN) is deposited and patterned to cover all areas except the waveguide core and the light emission region, which functions as a scattered and stray light absorber. Finally, a top layer of SiO_2 is deposited over the TiN. The device layers are transferred to a quartz substrate through wafer bonding, followed by the removal of the Si handle wafer. Further details on the fabrication process can be found in Supplementary Information Section 1.

The fabricated wafer is singulated into individual dies, which are then edge-polished for fibre or direct laser coupling. The fibre-attached device chip is aligned and bonded onto a commercial LCoS panel using ultraviolet-curable epoxy. A thin-film reflective polarizer with pressure-sensitive adhesive is affixed to the top side of the PIC chip, serving as a polarization analyser. For AR demonstration, the packaged PIC–LCoS sample is further aligned with a custom-designed projector lens and a geometrical waveguide combiner (Supplementary Information Sections 7–9).